Asian Journal of Chemistry; Vol. 37, No. 5 (2025), 1141-1150

ASIAN JOURNAL OF CHEMISTRY

https://doi.org/10.14233/ajchem.2025.33576

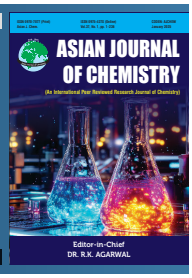

Silane Coupled E-Glass Fiber Reinforced Bismaleimide-Epoxy-Rochelle Salt Composites for High Dielectric Applications

K. Savitha Unnikrishnan[1], T. Sunil Jose[1,*], S. Dinoop Lal[1], K.J. Arun[2], P. Anju Rose Puthukkara[1], P. Martin Francis[1] and K.J. Rijoy[1]

[1]Department of Chemistry, St. Thomas' College, Thrissur-680001, India
[2]Department of Physics, Sree Kerala Varma College, Thrissur-680011, India

*Corresponding author: E-mail: suniljosestc@gmail.com

Received: 26 February 2025; *Accepted*: 4 April 2025; *Published online*: 30 April 2025; AJC-21981

A high performance bismaleimide (BMI)-epoxy-Rochelle salt (RS) composites reinforced with E-glass fiber (EGF) as well as silane coated unidirectional E-glass fiber (SC-EGF) were developed. The composite loaded with 2 wt.% of RS filler demonstrated maximum increment in dielectric constant as well as in mechanical properties. Composite with 3 wt.% of RS filler exhibited high dielectric strength indicating their adaptability for high voltage insulating applications. Dielectric constants and dielectric loss of the fabricated composites measured at higher frequencies (in GHz) using Vector Network Analyzer at room temperature was found to be highest for the BMI-Epoxy composite with 1 wt.% filler. Among the composites, the reinforced with SC-EGF exhibited significant increase in mechanical properties attributing to the interaction between matrix and silane functional groups on the glass fiber as evident through IR spectroscopy. The developed composite exhibiting low dielectric loss and high dielectric permittivity at room temperature can be applied in high dielectric applications.

Keywords: Polymer composites, Bismaleimide resin, Epoxy, Rochelle salt, Mechanical properties, Dielectric properties.

INTRODUCTION

Being one of the most important high performance thermosetting resins, bismaleimide resin (BMI) has several applications in electronics, radar [1], capacitors [2], stealth technologies [3], circuit boards [4], microelectronics *etc*. [5,6]. Different approaches like blending with rubber, thermoplastics, thermosets, reinforcement with glass fiber or carbon fiber, *etc.* may be adopted to overcome the brittle nature of the cured resin, epoxy resins are the widely used thermosetting matrix materials for high performance advanced composites. Epoxies are widely accepted in aerospace industry for the manufacture of most important composite parts because of its excellent mechanical properties, ease of manufacture and suitable service temperature [7]. BMI composites possess mechanical properties higher than epoxies and are more efficient than the corresponding epoxies in high temperature applications. In order to achieve both temperature performance of the BMI resin and the processing ease of epoxy resins, attempts have been made to prepare BMI-epoxy composites [8,9]. The thermal, mechanical and dielectric properties of the polymer composites mainly depend on the polymer matrix, size and weight percentage of the filler materials [10]. All these parameters are crucial for the fabrication of polymer composites and all these parameters should be optimized for the development of a novel polymer nanocomposite.

Sodium potassium tartrate tetrahydrate, also known as Rochelle salt (RS) or Seignette salt, utilized in phonograph pick-ups and microphones, was the identified piezoelectric material initially. Rochelle salt is highly soluble in water and deliquescent but in humid environments, transducers composed of this material may degrade. As the only known long-standing ferroelectric, it has numerous applications including as a laxative, in organic synthesis, in the silvering of mirrors, as a component of Fehling's solution, as an ingredient in Biuret reagent, *etc*. [11,12].

Rochelle salt was the compound in which ferroelectric behaviour was first recognized by Valasek [13]. Unusual dielectric constant was exhibited by Rochelle salt in ferroelectric

temperature from -40 ºC to +40 ºC. Levitskii *et al*. [14] studied the piezoelectric effect of Rochelle salt on the basis of Mitsui-type model and describes the dielectric relaxation and thermodynamic properties along with ferroelectric phase transition at the microscopic level in Rochelle salt.

The introduction of high dielectric permittivity materials in nanoscale into the polymer matrix could increase the dielectric constant of the polymer nanocomposites [15]. For high dielectric applications, the polymer composite should exhibit high dielectric permittivity, low dielectric loss and high break down strength [16-18]. High dielectric permittivity is highly desired for the dielectric materials used in the embedded capacitors and energy storage devices [19-21]. In order to enhance the dielectric properties of the BMI epoxy composites, suitable fillers with high dielectric constants are added [22].

In present work, the effect of incorporation of Rochelle salt (RS) filler into BMI-epoxy composites reinforced separately with E-glass fiber (EGF) and silane coated unidirectional E-glass fiber (SC-EGF) on the thermo-mechanical as well as dielectric properties is investigated. To the best of our knowledge, this is first report on the fabrication of Rochelle salt incorporated BMI-epoxy composites.

EXPERIMENTAL

Bismaleimide resin (BMI) was obtained from ABR Organics Ltd. Hyderabad, India. Epofine-1564 was procured from Fine Finish Organics Pvt. Ltd., Taloja, India. Rochelle salt (sodium potassium tartarate tetrahydrate, Sigma-Aldrich, India), E-Glass fibers (EGF) and silane coated E-Glass fibers (SC-EGF, Urja Products Pvt Ltd, India) were also purchased for this study.

Preparation of Rochelle salt crystals (RS): Mechanical ball milling based on the top-down method was used for producing metallic and ceramic materials. Rochelle salt crystals were ground well for a period of 4 h using a ball mill.

Fabrication of bismaleimide (BMI)-epoxy composites: Fabrication of both silane coupled E-glass fiber (SC-EGF) and E-glass fiber (EGF) reinforced BMI-epoxy composites with 1-5 wt.% of RS filler and without this filler were done using hand layup method followed by compression moulding, by maintaining 15:1.5 weight ratio of BMI and epoxy resin in all the composites [23].

Characterization: The chemical structure of the BMI resin, BMI-epoxy composites, RS crystals, interactions of the RS crystals in the composites were characterized using a Fourier transform infrared spectrometer (FTIR-ATR) IRAffinity-1S, Shimadzu, Japan. During the measurements transmission mode was selected and all the FTIR spectra were recorded in the range 4000-400 cm^{-1}. X-ray diffraction XRD analysis was done using X-ray diffractometer Aeris, PANalytical -United Kingdom with Cu-*K*α radiation (1.5406 Å wavelength), as the source. TGA-DSC was performed using Perkin-Elmer STA 6000, USA. The thermal scans were recorded at a heating rate of 20 ºC/min in nitrogen atmosphere between 30-750 ºC. The morphological studies were done by using the SEM images from JSM-6390LV, Japan. Elemental characterization of RS crystals was assessed by energy dispersive X-ray (EDX) analysis using Oxford XMX N, USA. The bending and tensile tests of the composites were studied as per ASTM standards using universal testing machine (UTM), Autograph AG-X plus, Shimadzu GmbH. Dielectric behaviour of samples was studied using Alpha–A-Analyzer, Germany in the range of 10^2-10^6 Hz. Dielectric permittivity at GHz frequencies of the fabricated samples was measured using vector network analyzer using different SRR's. As per ASTM D149 IEC 80243, Hipotronics-AC Dielectric test, Brewster, N.Y., USA, the AC Break down studies were performed on BMI/Epoxy RS composites.

RESULTS AND DISCUSSION

Thermal studies: The TGA curves of BMI resin, RS crystals, BMI-epoxy composite and BMI-epoxy composite with 2% RS filler are shown in Fig. 1. The TG analysis was done between 30 to 750 ºC at a heating rate of 20 ºC per min in nitrogen atmosphere. By comparative analysis of Fig. 1a(ii&iv), it is clear that BMI-epoxy composite with 2% RS filler have larger value of T_g, which may be due to the greater extent of cross links during curing and incorporation of RS filler strengthens the intermolecular forces. From the TGA curves (Fig. 1a), it is observed that BMI-epoxy composite with 2% RS have higher thermal stability compared to BMI resin and BMI-epoxy matrix, which may be due to the interaction of the dispersed RS filler with adjacent polymer matrix layers (Table-1).

TABLE-1
WEIGHT LOSS PERCENTAGES OF SAMPLES OBTAINED FROM THERMOGRAVIMETRIC CURVES

Compound	Stage	Temp. (ºC)	Weight loss (%)	Total weight loss (%)
BMI resin	I	47-383	4	66.0
	II	389-459	22	
	III	460-580	18	
	IV	588-722	22	
BMI-epoxy RS (2%) composite	I	45-357	5	44.0
	II	367-462	9	
	III	471-579	8	
	IV	591-717	22	
RS crystals	I	46-118	8	57.0
	II	121-241	16	
	III	251-291	19	
	IV	304-717	14	
BMI-epoxy composite without RS filler	I	118-433	8	93.4
	II	445-516	18	
	III	523-605	14	
	IV	611-736	53.4	

By comparing the three DSC curves, Fig. 1b(i-iii), the same endo curves could be observed around 558-563 ºC in all the three cases *i.e.*, 563 ºC for BMI resin, 559 ºC for RS crystals and 558 ºC for BMI-epoxy 2% RS composites. Glass transition temperature of BMI resin (288.85 ºC) was also identified from the DSC curve of the BMI resin.

Morphology of Rochelle salt crystals: SEM image of the Rochelle salt (Fig. 2a) revealed that the lattice is composed of polydispersed particles with diameter varying from 1-10 µm with sphere like morphology. The morphological variation of BMI resin as well as BMI-epoxy matrix is shown in Fig. 2(b-c).

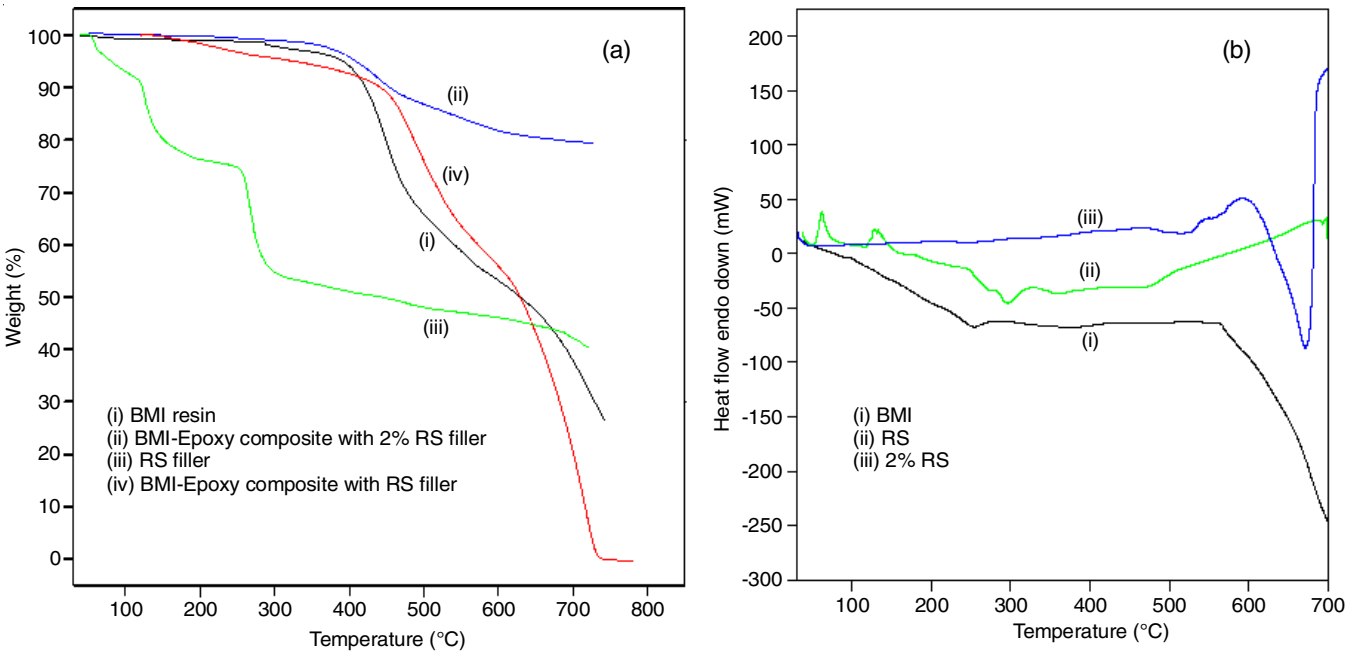

Fig. 1. (a) Thermograms of (i) BMI resin (ii) BMI-epoxy composite with 2% RS filler (iii) RS filler (iv) BMI-epoxy composite without RS filler (b) DSC curves of (i) BMI resin (ii) RS crystals (iii) BMI-epoxy composite with 2% RS filler

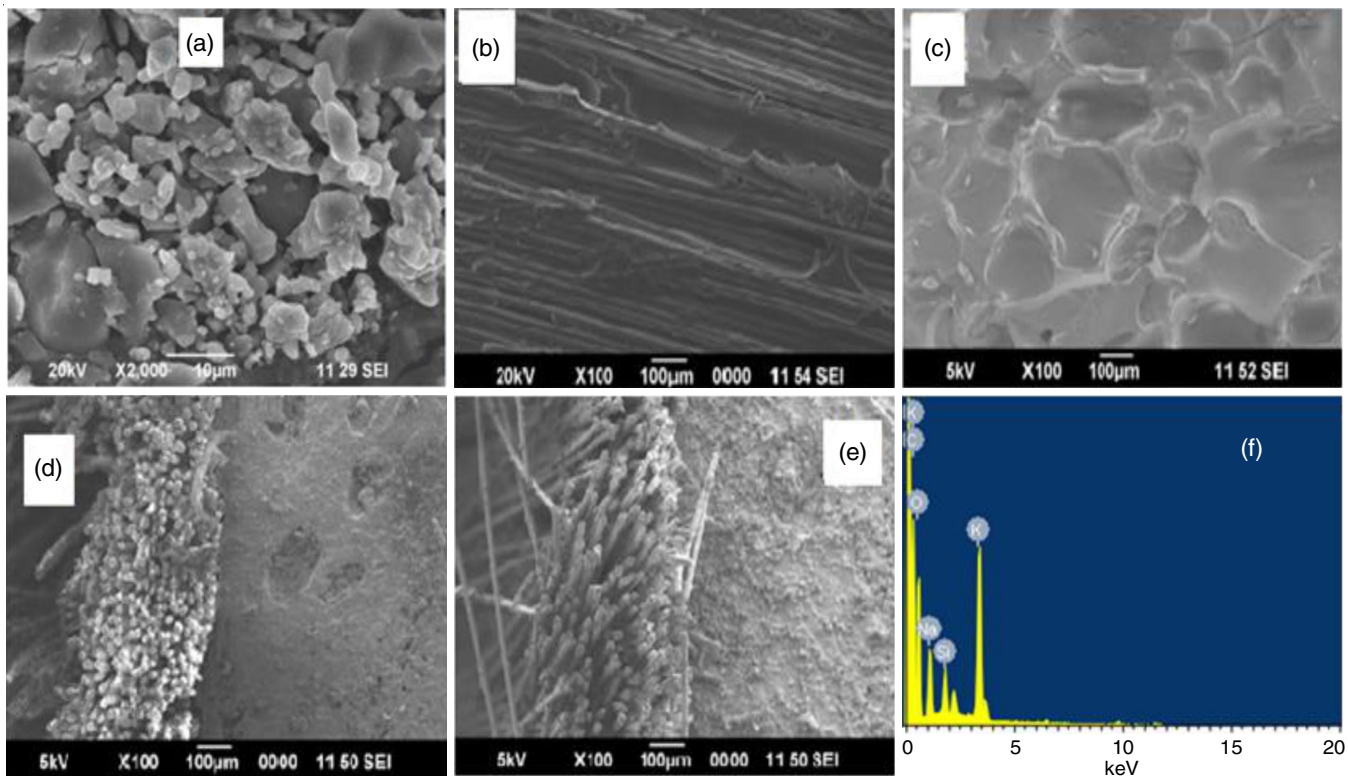

Fig. 2. SEM images of (a) RS crystals (b) BMI resin (c) BMI-epoxy composite without filler, cross sectional SEM images of BMI-epoxy nanocomposites with (d) 2% (e) 3% weights of RS particles and (f) EDAX of RS particles

The defective void like surface of BMI resin changes to more dense like structure in BMI-epoxy matrix indicating good compatibility between the blended polymers, which was also complemented by FTIR studies confirming the inter crosslinking between BMI and epoxy. Fig. 2d-e represents the cross-sectional SEM images of bismaleimide-epoxy composites loaded with 2 and 3 wt.% of RS particles. Bismaleimide-epoxy composite with 2 wt.% of RS particles possesses a uniform smooth surface that reveals the homogeneous dispersion of RS particles. EDAX pattern of RS particles (Fig. 2f) showed the presence of carbon, oxygen, sodium, potassium and silicon with atomic percentages of 56.40, 36.69, 2.77, 3.31 and 0.83, respectively.

From the diffractogram of RS, the maximum peak is obtained at 2θ = 16.19º and FWHM (β) = 0.13. Crystallite size (D) can be calculated using the Scherrer's formula:

$$D = \frac{k\lambda}{\beta\cos\theta} \quad (1)$$

where k = 0.89 (constant for spherical particle), λ is the wavelength of Cu-*K*α X-ray radiation used (0.15406 nm), β is the full width at half maximum (FWHM) of the most predominant peak obtained from diffractogram and θ is the angle of diffraction. The value of D was found to be approximately 61 nm.

EDAX spectra of the fabricated BMI-epoxy composite with 3 wt.% RS filler (Fig. 3a) confirmed the presence of carbon, oxygen, sodium and potassium in the sample. However, traces of silicon could also be observed in the spectra. Silicon has originated from the RS filler as evident from the EDAX of RS (Fig. 2f). EDAX mapping image (Fig. 3b) shows the dispersion of various elements throughout the composite matrix. Fig. 3c-e further show the dispersion of individual elements *i.e.* carbon, nitrogen and oxygen, respectively in the composite. The mapping image of these elements does not show any aggregation, indicating uniform dispersion of RS filler along BMI-epoxy composite matrix.

XRD studies: The semi-crystalline nature of BMI has changed to amorphous when modified with epoxy resin [Fig. 4b(i-ii)] primarily because of the intercalation of epoxy chains. Fig. 4a, represents the X-ray diffractogram of RS and the crystallite size of the RS as determined using Debye-Scherrer's equation was found to be ~61.02 nm. The XRD pattern gave several sharp peaks confirming the crystalline nature of RS. The XRD pattern of BMI-epoxy composite loaded with 2% RS as filler as shown in Fig. 4b(iii) indicated that RS loading into BMI-epoxy matrix has considerably altered the diffraction patterns of later. The single halo peak extending from 2θ values 10º to 30º, has splitted up into three peaks. In addition, some of the peaks corresponding to the crystal planes (410), (440), (512), *etc.* of RS are also visible. All these confirmed that crystallinity of BMI-epoxy has increased slightly upon RS loading (Table-2). These observations further point out the fact that RS was successsfully incorporated into BMI-epoxy composite matrix and an appreciable interaction existed between the composite matrix and RS filler.

FTIR studies: The FTIR spectrum of RS crystals recorded in the range 4000-400 cm^{-1} is shown in Fig. 5a. The strong C=O stretching band at 1610 cm^{-1} confirms the presence of carboxylate anion structure [24,25]. The strong peak at 1384

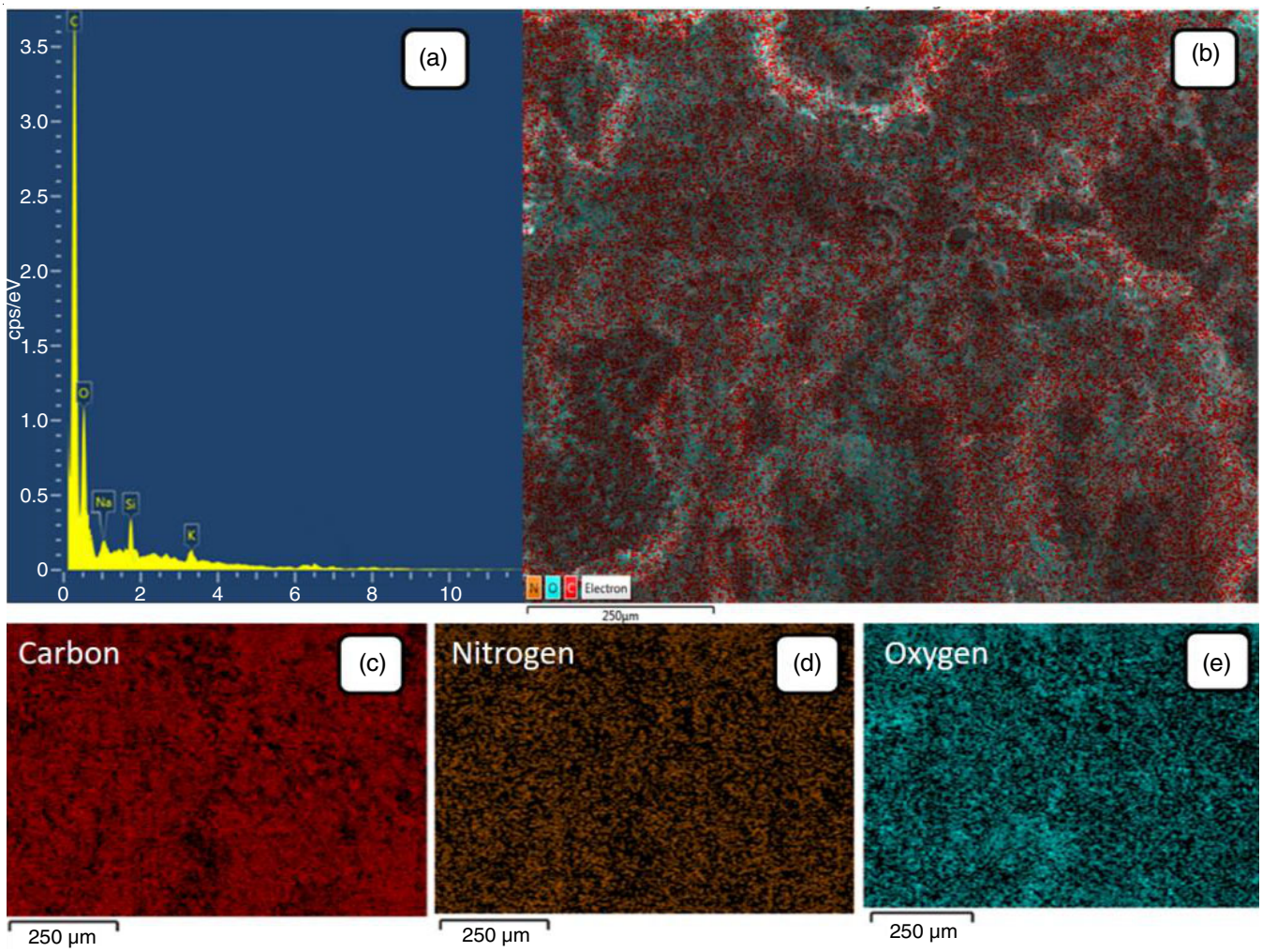

Fig. 3. EDAX spectra (a) and EDAX mapping (b, c and d) of bismaleimide-epoxy composite with 3 wt.% RS

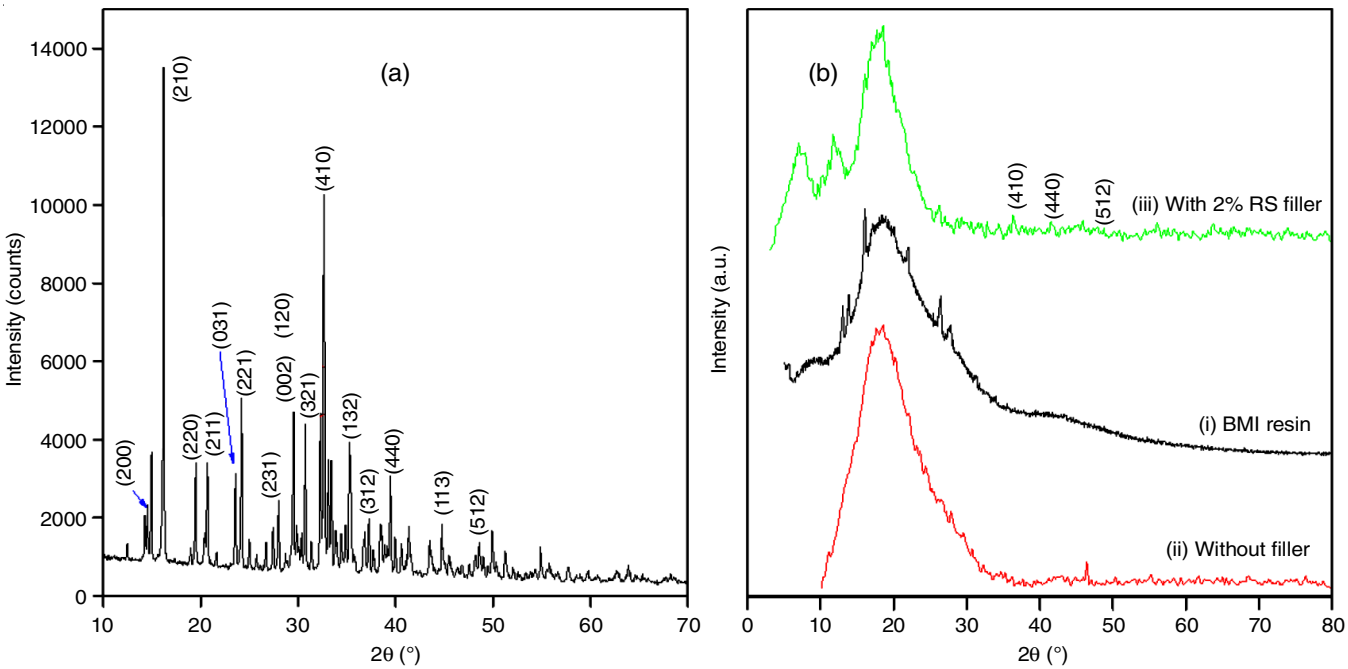

Fig. 4. X-ray diffraction pattern of (a) Rochelle salt (b) (i) BMI resin, BMI-epoxy composite (ii) without RS (iii) with 2% RS

TABLE-2
COMPARISON OF 2θ AND d VALUES IN BMI-EPOXY RS NANOCOMPOSITES WITH 2% AND 3% OF RS FILLER

Rochelle salt		BMI-epoxy composites with			
		2 wt.% RS filler		3 wt.% RS filler	
2θ	d (Å)	2θ	d (Å)	2θ	d (Å)
7.499	1.178	7.511	1.176	7.506	1.176
8.0209	1.104	8.004	1.1036	8.047	1.0977
18.0615	0.4908	18.07	0.4906	18.087	0.4901
18.4527	0.4805	18.471	0.4800	18.453	0.4793

Mapping of carbon (c) nitrogen (d) and oxygen (e).

cm^{-1} is due to COO^- symmetric vibration. Strong C-H stretching peaks are observed at 1118 cm^{-1} and 2328 cm^{-1} and the C-H stretching bands at 2137 (medium), 1240 (weak) and 1211 cm^{-1} (weak) were also observed. The strong and sharp C-O stretching peak at 982 cm^{-1} indicates less interaction with other groups in the crystal. The strong peak at 896 cm^{-1} corresponds to C-C stretching vibrations, whereas the medium peaks at 825, 707 and 613 cm^{-1} corresponds to the carboxylate anion. The low intensity O-H stretching vibration and strong O-H deformation appears at 3242, 3464 and 1051 cm^{-1}, respectively (Table-3).

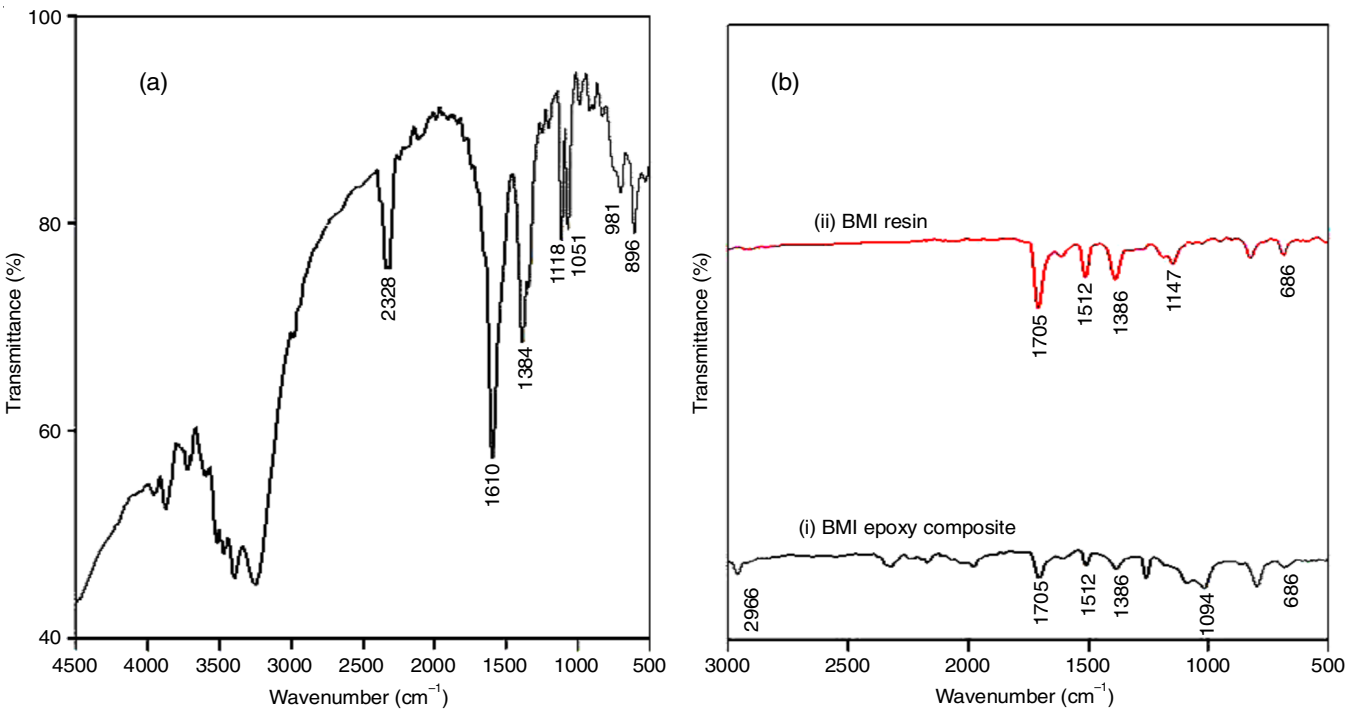

Fig. 5. FTIR analysis of (a) RS crystals (b) (i) BMI-epoxy composite (ii) BMI resin

TABLE-3
IMPORTANT IR STRETCHING
FREQUENCIES OF PURE RS CRYSTALS

Wavenumber (cm^{-1})	Assignment
3464.15w	O-H stretching
3242.34m	O-H stretching
2328.08s	C-H stretch
2137.13m	C-H stretch
1610.56vs	C=O stretch
1384.89s	C=O/-COO
1240.23w	C-H stretch
1211.29w	C-H stretch
1118.71s	C-H stretch
1051.20s	O-H deformation
981.76s	C-O stretching
896.89s	C-C stretch
825.53m	δ_{coo}
707.87m	τ_{coo}
613.36m	τ_{coo}

FTIR spectra recorded for pure BMI resin and BMI-epoxy composite are shown in Fig. 5b. Comparison of the peaks of FTIR spectra for pure BMI resin and BMI-epoxy composite reveals that the peaks corresponds to (i) the maleimide benzene ring and imide group at 686 and 1386 cm^{-1}, (ii) C=O group at 1705 cm^{-1} and (iii) C=C benzene ring at 1512 cm^{-1} show no shift in bands. The following shift in bands were observed during the fabrication of BMI-epoxy composites *viz.* (i) strong peak corresponds to C-N-C maleimide group at 1147 cm^{-1} shifted to 1094 cm^{-1} (medium) and (ii) peak corresponds to -C-H maleimide group at 3101 cm^{-1} shifted to 2965.57 cm^{-1}.

FTIR spectra of EGF and SC-EGF reinforced BMI-epoxy composites with varying weight percentages of RS filler (1-5%) are shown in Fig. 6. Comparative studies reveal that the characteristics peaks are not that much altered in differently reinforced BMI-epoxy RS composites. The IR peak for the oxirane ring of the epoxy resin is absent at 915 cm^{-1} in both BMI-epoxy composites with and without nanofiller [Fig. 6 & 5b(i)]. This suggests the possibility of ring opening and consequent crosslinking between epoxy and BMI. Absorption in the region 2850-3000 cm^{-1} corresponds to C-H stretching. The wavenumbers corresponding to epoxide ring vibrations (970, 862 and 1248 cm^{-1}) were also absent in the FTIR spectra of both BMI-epoxy composites with and without nanofiller further confirming the absence of epoxide ring. This indicates that during the fabrication of BMI-epoxy composites, inter crosslinking between BMI and epoxy resin occurred which proceeded through the ring opening of epoxy (oxirane ring) and formation of -N-CH(OH)CH_2- bonds between N of maleimide ring and –CH of epoxy resin [26].

Mechanical properties of BMI-epoxy RS composites: Fig. 7 represents the flexural and tensile measurements of the composites done as per ASTM standards. The flexural and tensile strength of BMI-epoxy RS composites were higher than that of BMI-epoxy composite without filler. When the wt.% of RS filler was different, the magnitude of tensile and flexural strength also varied and maximum value of tensile strength and flexural strengths was obtained when the wt.% of RS is 2%. This may be due to the uniform distribution of RS filler in the BMI-epoxy matrix with less agglomeration that facilitated

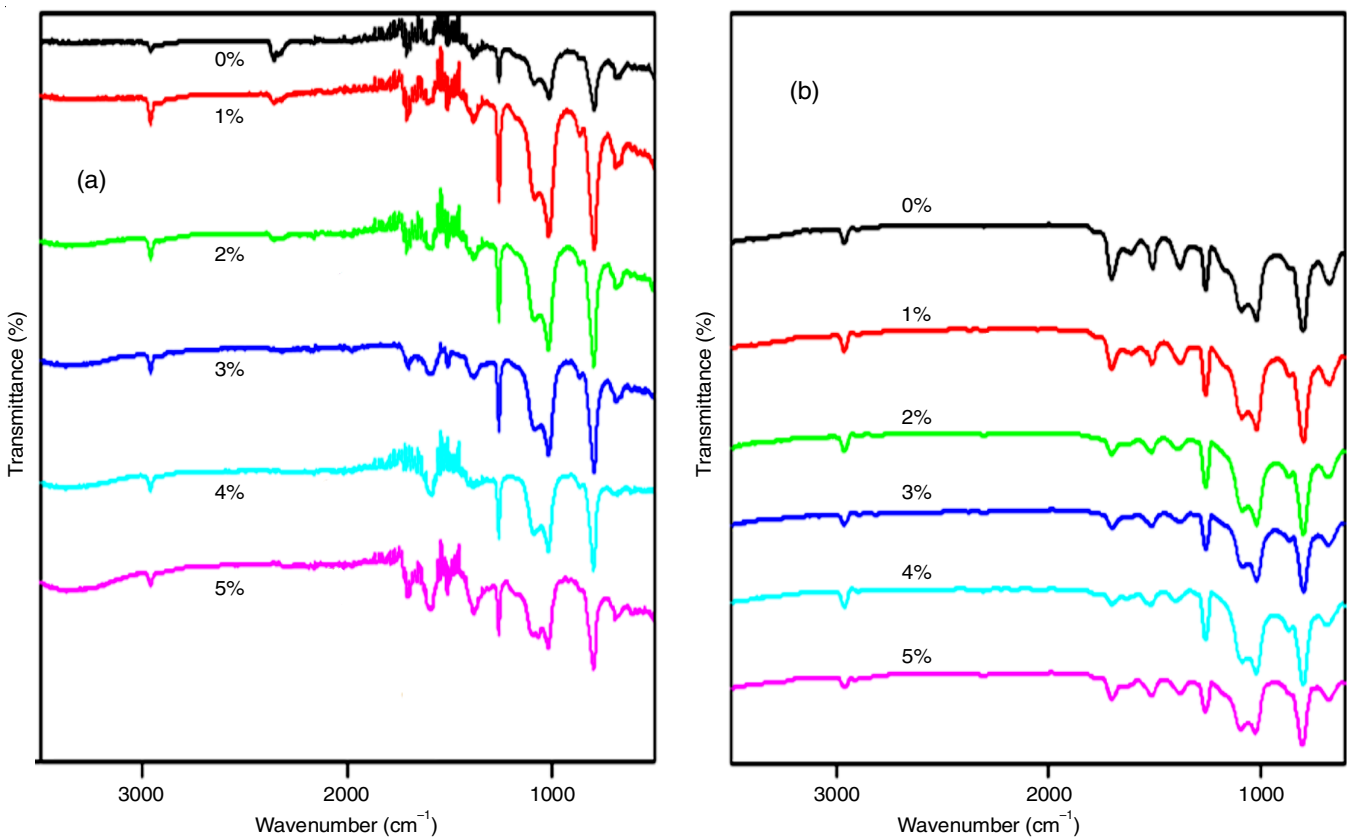

Fig. 6. FTIR analysis of the BMI-epoxy RS composites reinforced with (a) EGF (b) SC-EGF

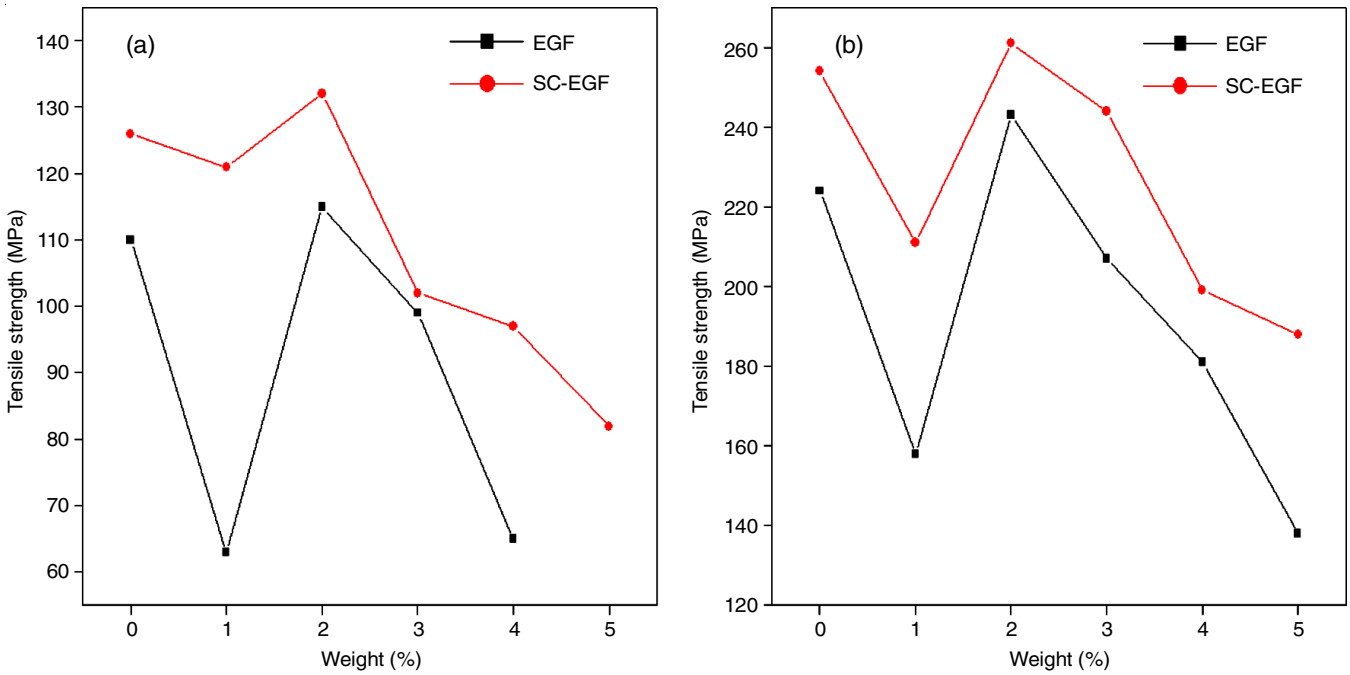

Fig. 7. Comparitive study of effect of wt.% of RS particles on (a) tensile strength and (b) flexural strength of BMI-epoxy RS composites reinforced with E-glass fiber (EGF) and silane coated E-glass fiber (SC-EGF)

comparatively strong interaction between the polymer matrix and filler, as evident from the SEM images (Fig. 2d-e).

The comparative analysis of the above test results showed that there is remarkable increase in the tensile and flexural strength of silane coated E-glass fiber reinforced composite, establishing the fact that there exists greater interaction between silane coated E-glass fiber and the polymer matrix [27].

Dielectric properties of BMI-epoxy RS composites

Dielectric permittivity: The studies were carried out at room temperature for the frequency range from 10^2 to 10^6 Hz. The plots of dielectric permittivity for the BMI-epoxy-RS composites with varying wt.% of RS crystals are shown in Fig. 8. The experimental values of dielectric constant showed a decreasing trend with increase in frequency as we expect in most of the dielectric materials that may be due to interfacial relaxation. Interfacial polarization have enough time to orient themselves in the direction of the alternating field [28]. Maximum values of dielectric constants are obtained for BMI-epoxy composite with 2 wt.% of RS filler [29,30]. Nanofiller content is responsible for the heterogeneity of the systems and the extended inter-

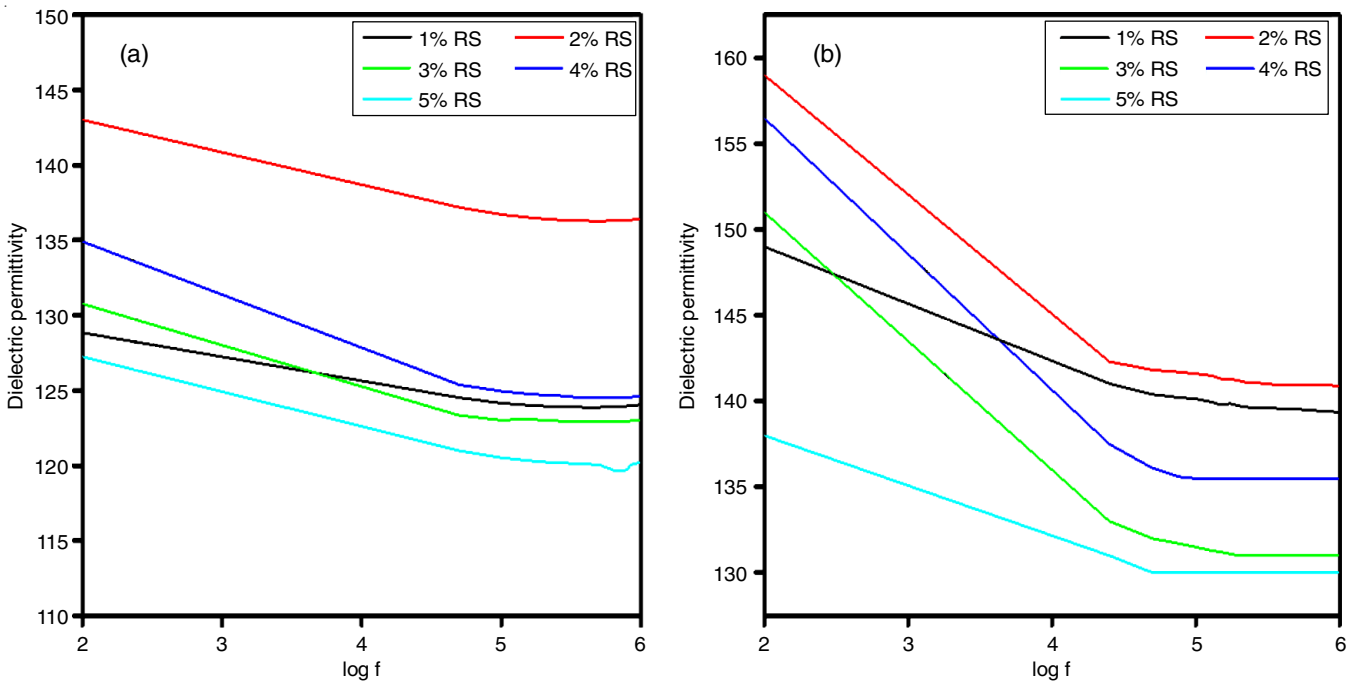

Fig. 8. Variation of relative permittivity with RS loadings of BMI-epoxy composites reinforced with (a) E-GF (b) SC-EGF

face. Space charges migrate under the influence of the field and accumulated at the interfaces where they form dipoles with enhanced inertia. This charge trapping procedure at the interface contributes to the dielectric response and permittivity [31].

Dielectric loss: Fig. 9 shows the variation of dielectric loss *versus* applied frequency for the differently loaded RS (1-5 wt.%) BMI-epoxy composites. At first, dielectric loss of the fabricated composites decreases with increase in frequency as expected due to the reduction of space charge polarization effect, reaches a minimum value and thereafter it increases with increase in frequency. At higher frequencies, due to the charge accumulation at polar grain boundaries, polarization increases resulting in increased mobility of charge carriers leading to high dielectric loss [32]. At very small ratio of RS (2%) the dielectric loss of the composite remained very low.

Dielectric properties at high frequencies: Dielectric permittivity and dielectric loss of the nanocomposites have been determined at GHz frequencies (Fig. 10) using vector network analyzer at room temperature [33]. Dielectric permittivity was found to be highest and dielectric loss was lowest for the BMI-epoxy nanocomposite with 1 wt.% nanofiller. When the wt.% of RS filler is above a certain value, the presence of agglomerated nanofiller at the interface may reduce the formation and accumulation of space charge. This may also leads to decrease the rate of charge trapping and so the dipoles get enough time to orient themselves which leads to decrease in dielectric permittivity. High frequency will disturb the already aligned dipoles in ferroelectric material and the reorientation of dipoles will not be easier in an external field and this leads to decrease in dielectric permittivity.

Breakdown voltage and dielectric strength: Dielectric breakdown strength of an insulating material depends on several factors like chemical structure, additives with different dielectric constant, structural irregularities, interfacial interactions between the polymer matrix and filler/additive, distortion of electric field due to the difference in dielectric permittivities of the polymer matrix and the filler, degree of crystallinity, *etc.* Fig. 11 represents the effect of wt.% of RS crystals on dielectric strength of BMI-epoxy-RS composites. The energy storage capacity and energy density of polymer nanocomposites depend upon the value of break down field strength. Glass fiber reinforced (E-GF and SC-EGF) BMI-epoxy-RS crystals with 3% of RS filler have better insulating properties. The increase in breakdown strength may be due to the synergic effect of uniform dispersion of the filler in BMI-epoxy matrix as well as the reduction in the mobility of the polymer chains as a result of interaction of Rochelle salt with BMI-epoxy matrix through hydrogen bonding.

Conclusion

In this research work, both E-glass fiber (EGF) and silane coated unidirectional E-glass fiber (SC-EGF) reinforced BMI-epoxy composites, BMI-epoxy composites with RS particles at different loadings were prepared and the effects of differently loaded RS filler on the mechanical, thermal and dielectric properties of BMI-epoxy composites were studied. Both EGF and

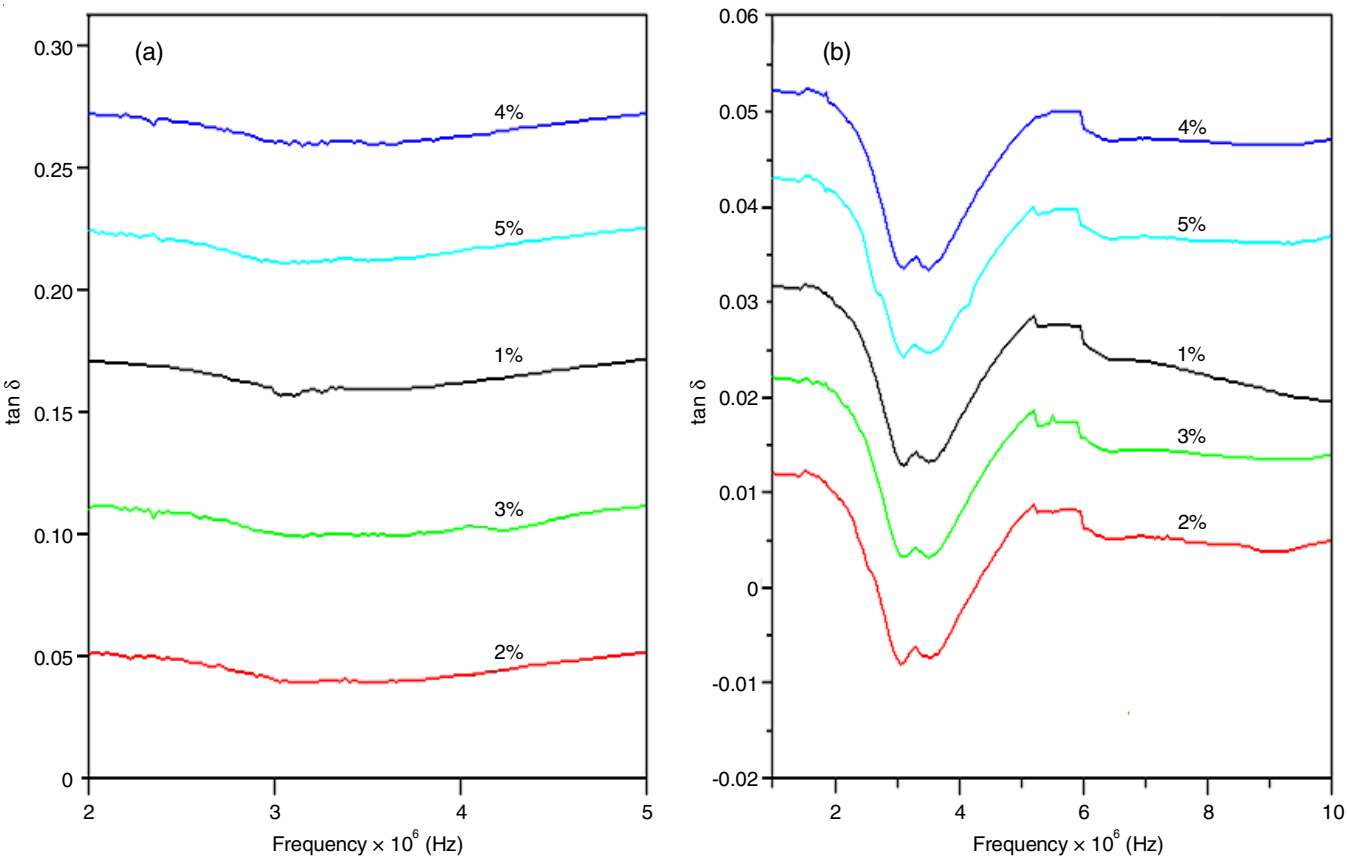

Fig. 9. Frequency -tan δ graph of BMI-epoxy RS composites reinforced with (a) EGF (b) SC-EGF

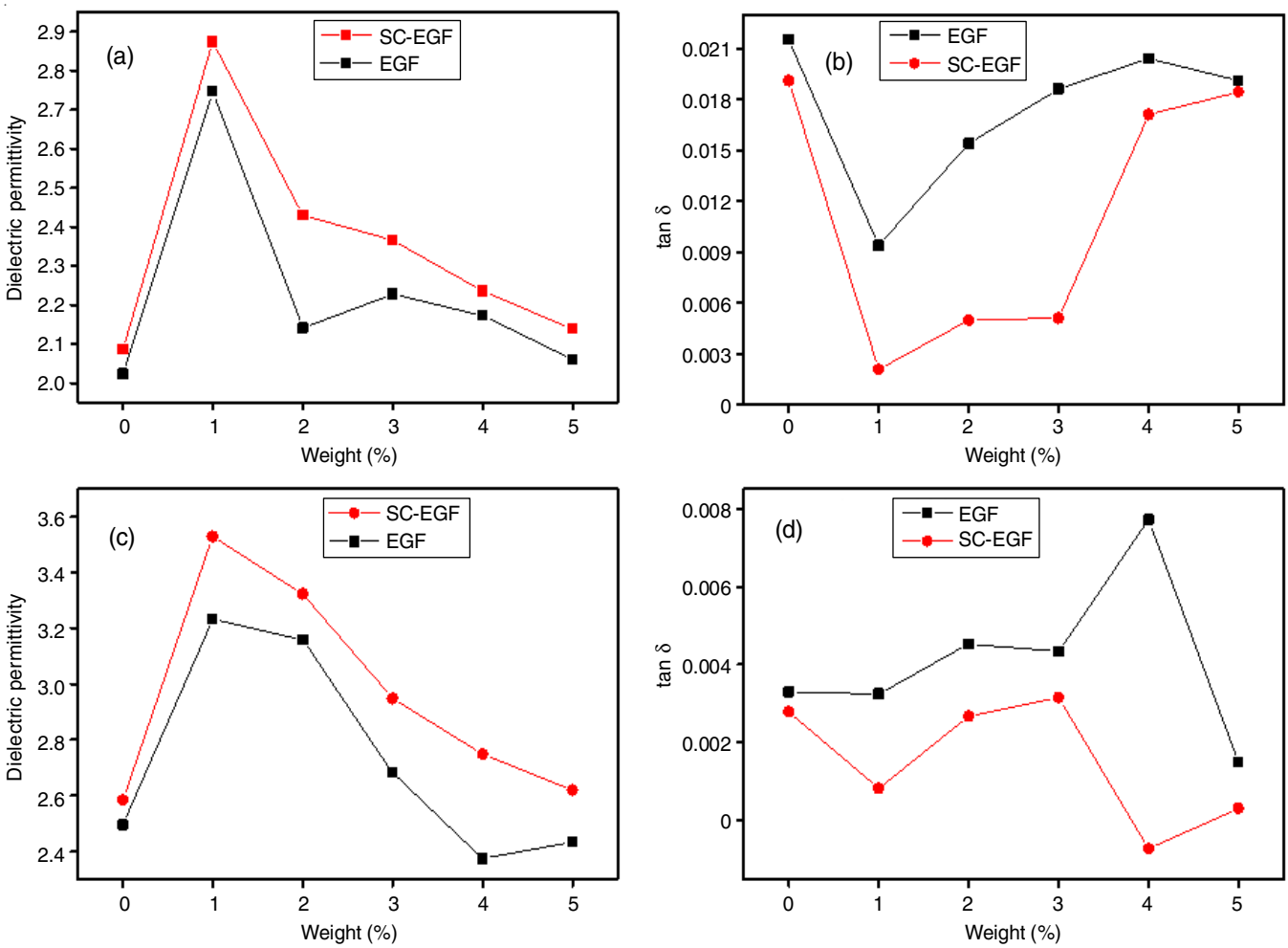

Fig. 10. Dielectric permittivity and tan δ of BMI epoxy RS composites with EGF and SC-EGF at frequency 3.42 GHz (a&b) and 5.68 GHz (c&d)

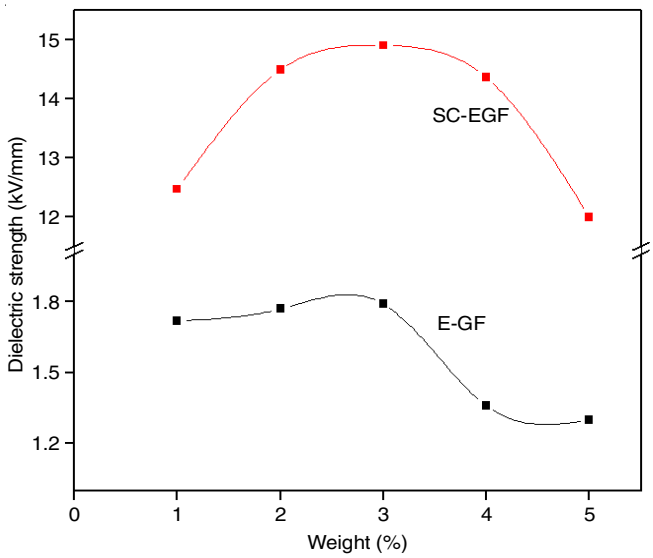

Fig. 11. Effect of wt.% of RS crystals of BMI epoxy composites reinforced with both EGF and SC-EGF on break down voltage

SC-EGF reinforced BMI-epoxy-RS composites with 3 wt.% of RS filler have better insulating properties and with 2 wt.% of RS filler have better dielectric and mechanical properties. The enhancement in both mechanical and dielectric properties may arise from the synergic effect of uniform dispersion of RS filler and comparatively strong interaction between the polymer matrix and RS filler. Tensile strength of BMI-epoxy composite with 2 wt.% RS nanofiller was increased 1.05 and 3.34 times both in EGF and SC-EGF reinforced composites whereas the flexural strength of the above composite was increased 1.085 and 4.24 times, respectively with EGF and SC-EGF reinforcement as compared to the composite without filler. The enhancement in breakdown voltage of BMI-epoxy composite with 2 wt.% RS nanofiller was found to be 1.12 and 3.88 times, respectively with EGF and SC-EGF reinforcement as compared to the composite without filler. This significant enhancement in tensile and flexural strength as well as in breakdown voltage may be due to greater interaction between SC-EGF and the BMI-epoxy matrix. Maximum value of dielectric constant and minimum value of dielectric loss is obtained for BMI-epoxy composite with 2 wt.% of RS filler. Among the differently reinforced composites the one with SC-EGF reinforced showed remarkable enhancement in both mechanical and dielectric properties that may be due to greater interaction between SC-EGF and the BMI-epoxy matrix. So these composites might be applied in high dielectric application devices.

ACKNOWLEDGEMENTS

The authors acknowledge SAIF-STIC, Cochin University of Science and Technology (CUSAT), India and National Institute of Science and Technology, Calicut, India for their valuable support.

CONFLICT OF INTEREST

The authors declare that there is no conflict of interests regarding the publication of this article.

REFERENCES

1. C.G. Jayalakshmi, A. Inamdar, A. Anand and B. Kandasubramanian, *J. Appl. Polym. Sci.*, **136**, 47241 (2019); https://doi.org/10.1002/app.47241
2. M. Kakimoto, A. Takahashi, T. Tsurumi, J. Hao, L. Li, R. Kikuchi, T. Miwa, T. Oono and S. Yamada, *Mater. Sci. Eng. B*, **132**, 74 (2006); https://doi.org/10.1016/j.mseb.2006.02.032
3. P.D. Mangalgiri, *Def. Sci. J.*, **55**, 175 (2005); https://doi.org/10.14429/dsj.55.1980
4. E.G. Fernandes, C. Tramidi, G.M. Di Gregorio, G. Angeloni and E. Chiellini, *J. Appl. Polym. Sci.*, **110**, 1606 (2008); https://doi.org/10.1002/app.28579
5. J. Hu, A. Gu, G. Liang, D. Zhuo and L. Yuan, *Express Polym. Lett.*, **5**, 555 (2011); https://doi.org/10.3144/expresspolymlett.2011.54
6. R.J. Iredale, C. Ward and I. Hamerton, *Prog. Polym. Sci.*, **69**, 1 (2017); https://doi.org/10.1016/j.progpolymsci.2016.12.002
7. R. Wazalwar, M. Sahu and A.M. Raichur, *Nanoscale Adv.*, **3**, 2741 (2021); https://doi.org/10.1039/D1NA00050K
8. R. Chandra and L. Rajabi, *J. Macromol. Sci. Part C Polym. Rev.*, **37**, 61 (1997); https://doi.org/10.1080/15321799708014733
9. L. Rajabi and G. Malekzadeh, *Iran. Polym. J.*, **15**, 447 (2006).
10. M.N. Alghamdi, *J. King Saud Univ. Eng. Sci.*, **34**, 361 (2022); https://doi.org/10.1016/j.jksues.2020.12.009
11. E. Lemaire, R. Moser, C.J. Borsa, H. Shea and D. Briand, *Procedia Eng.*, **120**, 360 (2015); https://doi.org/10.1016/j.proeng.2015.08.637
12. E. Lemaire, C. Ayela and A. Atli, *Smart Mater. Struct.*, **27**, 025005 (2018); https://doi.org/10.1088/1361-665X/aaa209
13. J. Valasek, *Ferroelectrics*, **2**, 239 (1971); https://doi.org/10.1080/00150197108234098
14. R.R. Levitskii, I.R. Zachek, T.M. Verkholyak and A.P. Moina, *Phys. Rev. B*, 67, 174112 (2003); https://doi.org/10.1103/PhysRevB.67.174112
15. Y. Thakur, T. Zhang, C. Iacob, T. Yang, J. Bernhol, L.Q. Chen, J. Runt and Q.M. Zhang, *Nanoscale*, **9**, 10992 (2017); https://doi.org/10.1039/C7NR01932G
16. T.T.M. Phan, N.C. Chu, V.B. Luu, H.N. Xuan, D.T. Pham, I. Martin and P. Carrière, *J. Sci. Adv. Mater. Devices*, **1**, 90 (2016); https://doi.org/10.1016/j.jsamd.2016.04.005
17. A. Gu, *Compos. Sci. Technol.*, **66**, 1749 (2006); https://doi.org/10.1016/j.compscitech.2005.11.001
18. P. Barber, S. Balasubramanian, Y. Anguchamy, S. Gong, A. Wibowo, H. Gao, H.J. Ploehn and H.-C. Zur Loye, *Materials*, **2**, 1697 (2009); https://doi.org/10.3390/ma2041697
19. Q. Jia, X. Huang, G. Wang, J. Diao and P. Jiang, *J. Phys. Chem. C*, **120**, 10206 (2016); https://doi.org/10.1021/acs.jpcc.6b02968
20. X. Zhu, J. Yang, D. Dastan, H. Garmestani, R. Fan and Z. Shi, *J. Compos. Part A*, **125**, 105521 (2019); https://doi.org/10.1016/j.compositesa.2019.105521
21. B. Zhao, M. Hamidinejad, C. Zhao, R. Li, S. Wang, Y. Kazemi and C.B. Park, *J. Mater. Chem. A*, **7**, 133 (2019); https://doi.org/10.1039/C8TA05556D
22. J. Hu, A. Gu, G. Liang, D. Zhuo and L. Yuan, *Express Polym. Lett.*, **5**, 555 (2011); https://doi.org/10.3144/expresspolymlett.2011.54
23. K.S. Unnikrishnan, T.S. Jose, S.D. lal and K.J. Arun, *Polym. Test.*, **87**, 106505 (2020); https://doi.org/10.1016/j.polymertesting.2020.106505
24. R. Bhattacharjee, Y.S. Jain, G. Raghubanshi and H.D. Bist, *J. Raman Spectrosc.*, **19**, 51 (1988); https://doi.org/10.1002/jrs.1250190108
25. M.J. Uddin, T.R. Middya and B.K. Chaudhuri, *Curr. Appl. Phys.*, **13**, 461 (2013); https://doi.org/10.1016/j.cap.2012.09.016
26. P. Maity, S.V. Kasisomayajula, V. Parameswaran, S. Basu and N. Gupta, *IEEE Trans. Dielectr. Electr. Insul.*, **15**, 63 (2008); https://doi.org/10.1109/T-DEI.2008.4446737
27. S.Y. Kanag, Y.K. Anandan, P. Vaidyanath and P. Baskar, *Gradjevinar*, **68**, 697 (2016); https://doi.org/10.14256/JCE.1335.2015
28. L. Wan, X. Zhang, G. Wu and A. Feng, *High Volt.*, **2**, 167 (2017); https://doi.org/10.1049/hve.2017.0056
29. A. Mansingh and S.S. Bawa, *Phys. Status Solidi, A Appl. Res.*, **21**, 725 (1974); https://doi.org/10.1002/pssa.2210210239
30. C.B. Sawyer and C.H. Tower, *Phys. Rev.*, **35**, 269 (1930); https://doi.org/10.1103/PhysRev.35.269
31. G.C. Manika and G.C. Psarras, *Express Polym. Lett.*, **13**, 749 (2019); https://doi.org/10.3144/expresspolymlett.2019.63
32. P.R. Das, L. Biswal, B. Behera and R.N.P. Choudhary, *Mater. Res. Bull.*, **44**, 1214 (2009); https://doi.org/10.1016/j.materresbull.2009.01.013
33. S.P. Chakyar, S. K. Simon, C. Bindu, J. Andrews and V.P. Joseph, *J. Appl. Phys.*, **121**, 054101 (2017); https://doi.org/10.1063/1.4975111